The Company of Biologists

RESEARCH ARTICLE

Desmoglein 2 mutation provokes skeletal muscle actin expression and accumulation at intercalated discs in murine hearts

Sebastian Kant[1], Benjamin Freytag[1], Antonia Herzog[1], Anna Reich[1], Rudolf Merkel[2], Bernd Hoffmann[2], Claudia A. Krusche[1] and Rudolf E. Leube[1,*]

ABSTRACT

Arrhythmogenic cardiomyopathy (AC) is an incurable progressive disease that is linked to mutations in genes coding for components of desmosomal adhesions that are localized to the intercalated disc region, which electromechanically couples adjacent cardiomyocytes. To date, the underlying molecular dysfunctions are not well characterized. In two murine AC models, we find an upregulation of the skeletal muscle actin gene (*Acta1*), which is known to be a compensatory reaction to compromised heart function. Expression of this gene is elevated prior to visible morphological alterations and clinical symptoms, and persists throughout pathogenesis with an additional major rise during the chronic disease stage. We provide evidence that the increased *Acta1* transcription is initiated through nuclear activation of the serum response transcription factor (SRF) by its transcriptional co-activator megakaryoblastic leukemia 1 protein (MKL1, also known as MRTFA). Our data further suggest that perturbed desmosomal adhesion causes *Acta1* overexpression during the early stages of the disease, which is amplified by transforming growth factor β (TGFβ) release from fibrotic lesions and surrounding cardiomyocytes during later disease stages. These observations highlight a hitherto unknown molecular AC pathomechanism.

KEY WORDS: Arrhythmogenic right ventricular cardiomyopathy, Intercalated disc, Desmoglein, Myocardin-related transcription factor A, Serum response factor

INTRODUCTION

Arrhythmogenic cardiomyopathy (AC), which is also referred to as arrhythmogenic right ventricular cardiomyopathy/dysplasia (ARVC/D), is an inherited heart disease (Basso et al., 2011; Hoorntje et al., 2017). It is characterized by life-threatening arrhythmia, often at early disease stages with only little or no morphological alterations, and by extensive fibrofatty or fibrous replacement of myocardium at later stages (Basso et al., 2011). The majority of patients with pathogenic gene modifications carry mutations in the desmosomal components desmoglein 2, desmocollin 2, plakophilin 2, plakoglobin and desmoplakin (Agullo-Pascual et al., 2014; Basso et al., 2011; Delmar and McKenna, 2010; Groeneweg et al., 2015). Desmosomes are Ca^{2+}-dependent cell–cell contacts that serve as anchorage sites for

the desmin intermediate filament cytoskeleton (for a recent review, see Nekrasova and Green, 2013). In the heart, they are part of the intercalated disc structure that mechanically and electrochemically couples adjacent cardiomyocytes including, besides desmosomes, actin-anchoring fasciae adhaerentes and ion-permeable gap junctions. To describe this complex situation, mixed structural units have been proposed that are referred to as area composita (Franke et al., 2006) or connexome (Agullo-Pascual et al., 2014).

To examine the largely unknown molecular mechanisms of AC pathogenesis, murine models have been established (Lodder and Rizzo, 2012; Rickelt and Pieperhoff, 2012), thereby enabling the investigation of early disease stages and the monitoring of disease progression. Mice with mutations in the desmosomal cadherin desmoglein 2 (DSG2) develop a cardiomyopathy (Kant et al., 2015; Krusche et al., 2011; Pilichou et al., 2009), which shares features with AC patients carrying mutations in the desmoglein 2 gene (*DSG2*) (Awad et al., 2006; Bauce et al., 2010; Pilichou et al., 2006; Syrris et al., 2007). A knock-in mouse that we recently described produces a mutant desmoglein 2 polypeptide (DSG2^{MT}) with a deletion in the extracellular domains EC1 and EC2, which are implicated in intercellular adhesion of desmosomal cadherins (Krusche et al., 2011; Tariq et al., 2015). Mice carrying two mutant *Dsg2* alleles (*Dsg2$^{mt/mt}$*) are born apparently healthy but develop cardiomyopathy from 2 weeks onward. Cardiomyocyte necrosis and immune cell invasion occur in myocardial lesions that appear between 2 and 6 weeks. Afterwards, the inflammatory reaction subsides and connective tissue replaces the necrotic tissue leading to scar formation (Kant et al., 2015, 2012; Krusche et al., 2011). A very similar phenotype is observed in cardiomyocyte-specific *Dsg2* knockout (cKO; *Dsg2$^{cKO/cKO}$*) mice (Kant et al., 2015).

The goal of the current study was to identify and characterize the early changes of gene transcription prior to overt morphological alterations in the hearts of *Dsg2*-mutant mice. Through a transcript analysis, we found that the expression of α1-skeletal muscle actin (*Acta1*) was increased in the myocardium of *Dsg2$^{mt/mt}$* and *Dsg2$^{cKO/cKO}$* mice prior to lesion formation, and show that *Acta1* expression further increases during disease progression with a conspicuous accumulation of F-actin at intercalated discs. Our further observations suggest that the early upregulation of *Acta1* is linked to impaired mechanical cardiomyocyte coupling, while the later increase is caused by transforming growth factor β (TGFβ) production in fibrotic myocardial lesions and adjacent cardiomyocytes. We present evidence that both stimuli may act through the transcriptional co-activator megakaryoblastic leukemia 1 protein MKL1 (also referred to as myocardin-related transcription factor A; MRTFA) on serum response factor (SRF)-dependent gene expression, which has been shown to be involved in cardiac hypertrophy (Kuwahara et al., 2010).
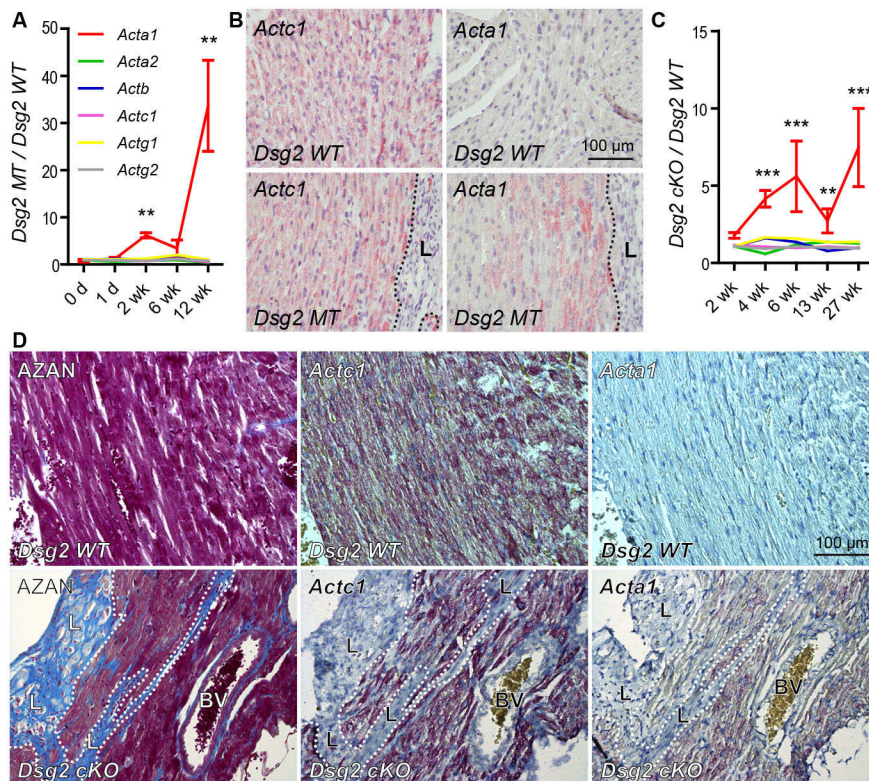
Journal of Cell Science

Fig. 1. *Acta1* mRNA expression is increased in the *Dsg2mt/mt* and *Dsg2cKO/cKO* hearts. (A) The graph shows ratios of mRNA expression levels for skeletal muscle actin *Acta1*, cardiac actin *Actc1*, smooth muscle actins *Acta2* and *Actg2* and cytoplasmic actins *Actb* and *Actg1* in *Dsg2mt/mt* (*Dsg2 MT*) versus wild-type (*Dsg2 WT*) mice [*n*=3 at day of birth (0d) and *n*=4 at all other time points given in days (d) or weeks (wk) after birth]. Housekeeping controls for normalization were: *Hprt*, *Tbp* and *Hmbs*. (B) *In situ* hybridization detecting *Actc1* and *Acta1* mRNA (red dotted signal) in hematoxylin-stained tissue sections of wild-type and *Dsg2mt/mt* myocardium (*n*=3). Note the strong and even *Actc1* distribution in the mutant and wild type, and the elevated and prominent *Acta1* mRNA expression next to the signal-free fibrotic lesion (L). Scale bar: 100 µm (same magnification in all images). (C) The graph depicts qRT-PCR results detecting actin isoforms (same denotations as in A) in *Dsg2cKO/cKO* (*Dsg2 cKO*) hearts in comparison to wild-type controls (housekeeping controls for normalization: *Tbp* and *Hprt*). A two-way ANOVA was used to calculate statistics for A and C. (D) *In situ* hybridization (same denotations as in B) detecting *Actc1* and *Acta1* mRNA in sections of wild-type and *Dsg2cKO/cKO* hearts together with serial azan-stained (AZAN) control sections on the left to delineate collagen-rich lesions (broken lines). BV, blood vessel. Scale bar: 100 µm (same magnification in all images). **P≤0.01; ***P≤0.001.

RESULTS

Expression of *Acta1* mRNA is increased in *Dsg2* mutant myocardium

To identify early changes in gene expression that are caused by *Dsg2* mutation, transcriptome profiles of heart tissue were determined for 2-week-old, macroscopically normal-appearing hearts of *Dsg2mt/mt* mice and compared to those of matched hearts obtained from *Dsg2wt/wt* and *Dsg2mt/wt* mice (*n*=3 in each instance). Only 35 genes were upregulated and 14 genes were downregulated in *Dsg2mt/mt* mice by a factor of 1.5 or more. Of those, ten showed a more than 1.5-fold increase and five a more than 1.5 fold decrease in *Dsg2mt/wt* mice (Table S1). The top candidate gene was *2210407C18Rik* with a 3.34-fold mRNA increase in the homozygous mutants and a 2.92-fold increase in the heterozygous animals. It encodes a poorly characterized epithelial cell surface protein that has been implicated in epithelial growth and differentiation (Kritzik et al., 2010). Its function in the heart is unknown. The second highest increase of gene transcription was observed for *Acta1*. A 1.70-fold increase was detected in heterozygous *Dsg2mt/wt* mice, and a 3.09-fold increase in homozygous *Dsg2mt/mt* mice. Interestingly, *Acta1* expression has been shown to be altered in various cardiac pathologies of rodents and humans (Driesen et al., 2009; Schiaffino et al., 1989; Schwartz et al., 1986; Stilli et al., 2006; Suurmeijer et al., 2003).

Quantitative reverse transcription PCR analyses (qRT-PCR) were subsequently performed to validate the altered mRNA expression of *Acta1* and to examine mRNA expression of all six actin isoforms at different time points after birth (Fig. 1A). Actin isoform mRNA expression was indistinguishable between mutant and wild type up to 1 day after birth. In 2-week-old animals, however, the level of *Acta1* mRNA was consistently increased in the mutant hearts (6.18-fold). By 6 weeks, the increase in *Acta1* expression had diminished slightly (3.45-fold) but was increased considerably by 12 weeks

(33.67-fold increase). In contrast, all other actin isoforms stayed at basal wild-type levels.

To substantiate these observations, we performed qRT-PCR of *Acta1* expression in a second AC mouse model, namely, *Dsg2cKO/cKO* mice (Kant et al., 2015). A similar expression profile emerged (Fig. 1C); *Acta1* mRNA levels started to increase selectively at 2 weeks with a transient peak at 6 weeks and considerable further increase during later disease stages.

In situ hybridization experiments were then performed to investigate the spatial relationship between elevated *Acta1* mRNA expression and lesion formation. *Acta1* mRNA was almost undetectable in the wild-type myocardium (Fig. 1B, upper right) but quite abundant in cardiomyocytes of *Dsg2mt/mt* hearts with highest expression levels in the vicinity of fibrotic lesions (Fig. 1B, lower right). A similar situation was encountered in *Dsg2cKO/cKO* mice (Fig. 1D). As expected, cardiac *Actc1* mRNA, which served as positive control, was evenly and strongly detectable in cardiomyocytes of wild-type, *Dsg2mt/mt* and *Dsg2cKO/cKO* animals (Fig. 1B, left panel; Fig. 1D, middle panel).

Pronounced F-actin accumulations occur at altered intercalated discs close to fibrotic lesions

Immunofluorescence staining was performed to examine actin protein expression. By using commercial antibodies, which presumably react selectively with ACTA1 (see below), sarcomeric staining was observed in wild-type and *Dsg2mt/mt* heart (Fig. 2A–C). In addition, increased immunoreactivity was noted at intercalated discs of cardiomyocytes next to fibrotic lesions in 12-week-old and older mice (Fig. 2C; Fig. S1B′). The increased immunoreactivity overlapped in part with anti-desmoplakin and anti-DSG2 immunofluorescence, and was restricted to the adjacent sarcomere (Fig. 2C′,C″; Fig. S1B,B″). Identical staining patterns were detected in *Dsg2cKO/cKO* mice (Fig. S1D–D″) and with anti-ACTC1 antibodies
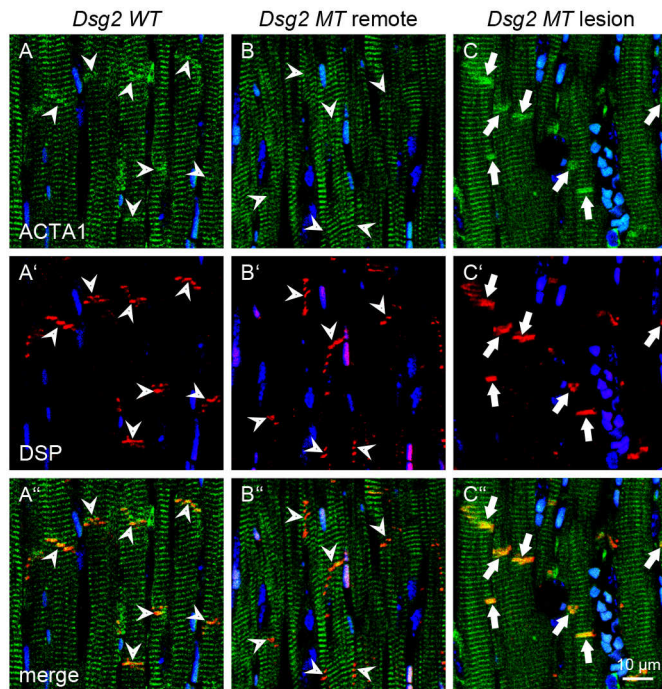
Fig. 2. Actin accumulates at intercalated discs of cardiomyocytes next to fibrotic lesions in *Dsg2mt/mt* myocardium. (A–C″) Double immunofluorescence microscopy detecting ACTA1 (green, top panel) and desmoplakin (DSP, red, middle panel; merged images in bottom panel) in wild-type (*Dsg2 WT*) and *Dsg2mt/mt* myocardium (*Dsg2 MT*; *n*=6 for each group; 12-week-old). Note the ACTA1 accumulation around desmoplakin-positive intercalated discs (white arrows) in a region close to a lesion which is not seen in remote areas of the mutant myocardium or in the wild type (arrowheads). Scale bar: 10 μm (same magnification in all images).

(Fig. S2). The latter suggest that the actin accumulations at intercalated discs most likely contain both ACTA1 and ACTC1. We would like to point out, however, that despite the presumed and reported antibody specificity (Franke et al., 1996; Moll et al., 2006), cross-reactivity cannot be fully excluded. This may be especially true for anti-ACTA1 antibodies, because a very low amount of ACTA1 epitopes competes with very large amounts of ACTC1 epitopes that are several orders of magnitude more abundant. Lack of specificity is also suggested by the *in situ* hybridization data depicted in Fig. 1, which clearly showed an enrichment of *Acta1* mRNA in perilesional regions that was not detected with the anti-ACTA1 antibodies.

Staining with fluorescence-labeled phalloidin confirmed actin accumulations at intercalated discs in perilesional areas and furthermore showed that they contain F-actin (Fig. 3). In addition, immunolocalization experiments revealed changes in the distribution of the desmosomal proteins desmoplakin and DSG2, and of the adherens junction protein cadherin 2 (CDH2) next to the conspicuous actin accumulations (Fig. 2C–C″, Fig. 3D–D″; Fig. S1B–B″,D–D″, Fig. S2C–C″). The respective signals were more homogenous and less restricted than the typically dotted and concise signals in the wild type (Fig. 2A′, Fig. 3A′; Fig. S1A″, Fig. S1C″, Fig. S2A′), in 2-week-old mutants without visible lesions (Fig. 3B′) and in remote areas of mutant myocardium with lesions (Fig. 2B′; Fig. S2B′). These observations indicate changes in intercalated disc structure and the arrangement of its molecular components in lesioned *Dsg2* mutant myocardium.

Tgfb mRNA is isoform and cell type specifically increased upon myocardial lesion formation

To examine reasons for altered actin mRNA and protein expression in perilesional areas, expression of the *Tgfb* isoforms was analyzed (Fig. 4). This was undertaken because it is known that TGFβ stimulates *Acta1* expression in cardiomyocytes through distinct serum response elements in the *Acta1* promoter (MacLellan et al., 1994; Parker et al., 1990, 1992). We therefore first studied whether *Tgfb1* expression is increased in lesions and/or in perilesional regions of *Dsg2mt/mt* hearts. By *in situ* hybridization, we could localize *Tgfb1* mRNA predominantly in fibrotic lesions of 12-week-old mice (Fig. 4A, right panels). In support of this finding, qRT-PCR assessment uncovered
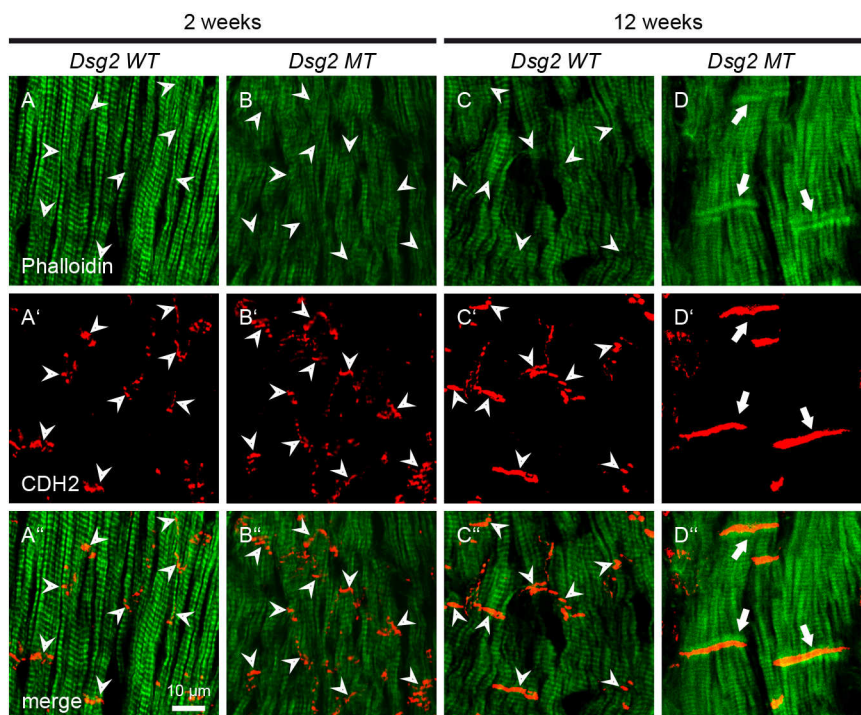

Fig. 3. F-actin accumulates at intercalated discs in *Dsg2mt/mt* cardiomyocytes after lesion formation. (A–D) F-actin staining with Alexa 488–phalloidin, (A′–D′) cadherin 2 (CDH2) immunostaining, and (A″–D″) overlay of phalloidin and CDH2 staining in the myocardium of 2-week-old (*n*=3) and 12-week-old (*n*=4) wild-type (*Dsg2 WT*) and *Dsg2mt/mt* mice (*Dsg2 MT*). Note the accumulation of F-actin around cadherin 2-positive intercalated discs in cardiomyocytes of 12-week-old mice (white arrows) but not in 2-week-old *Dsg2* mutants or wild-type hearts (arrowheads). Note also the less punctate and more diffuse distribution of CDH2 in actin-enriched intercalated discs. Scale bar: 10 μm (same magnification in all images).
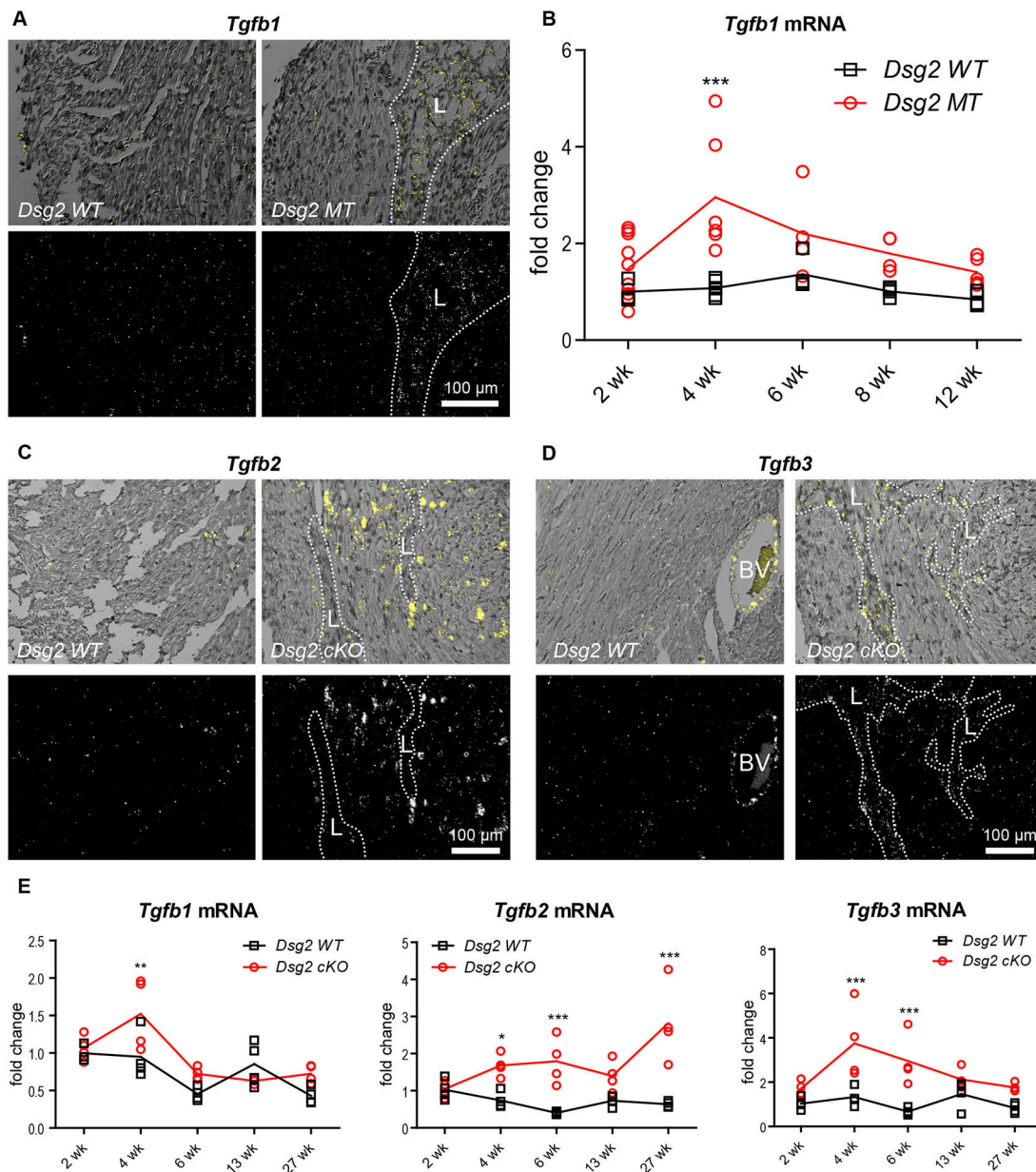
Fig. 4. *Tgfb* mRNA expression is upregulated in *Dsg2^mt/mt* and *Dsg2^cKO/cKO* hearts with fibrotic lesions. (A) Detection of *Tgfb1* mRNA (*n*=3) in wild-type (*Dsg2 WT*) and *Dsg2^mt/mt* (*Dsg2 MT*) myocardium by *in situ* hybridization. The images show bright field micrographs (top) of hematoxylin-stained tissue sections and corresponding dark field recordings (bottom). Note the high signal intensity (yellow dots in bright field images) within a lesion of the mutant heart (demarcated by dotted lines). Scale bar: 100 µm (same magnification in all images). (B) Dot plot depicting the time course of qRT-PCR detecting *Tgfb1* mRNA in wild-type and *Dsg2^mt/mt* hearts (*n*≥4 for each). Housekeeping control: *Hmbs*. Statistics: two-way ANOVA followed by a Bonferroni post hoc test. (C,D) Detection of *Tgfb2* and *Tgfb3* in sections of 26-36-week-old wild-type control and *Dsg2^cKO/cKO* (*Dsg2 cKO*)-mutant murine hearts (wild type *n*=3; mutant *n*=9). Note the increase of *Tgfb2* in cardiomyocytes next to lesions and of *Tgfb3* within lesions in the mutant hearts. Corresponding images of AZAN-stained serial sections are given in Fig. S5 and RGB color images of *in situ* hybridized heart tissue sections are given in Fig. S4. Scale bar: 100 µm (same magnification in all images). (E) Time course of qRT-PCRs detecting all *Tgfb* isoforms in *Dsg2^cKO/cKO* hearts (*n*=4). Housekeeping controls: *Tbp* and *Hprt*. Statistics: two-way ANOVA followed by a Bonferroni post hoc test. *P≤0.05; **P≤0.01; ***P≤0.001.

significantly increased levels of *Tgfb1* in *Dsg2^mt/mt* and also in *Dsg2^cKO/cKO* mutant hearts with fibrotic lesions at 4 weeks (Fig. 4B,E), that is, at a time when lesion formation is initiated. It subsequently reduced to near wild-type levels (Fig. 4B,E). Determination of *Tgfb2* and *Tgfb3* mRNA expression patterns revealed a more protracted elevation extending into the chronic disease phase (Fig. 4E; Fig. S3). *In situ* hybridization further showed that the increase in *Tgfb3* mRNA is most likely due to increased synthesis within newly formed and fibrotic lesions (Fig. 4D), whereas *Tgfb2* mRNA was considerably

upregulated in perilesional cardiomyocytes (Fig. 4C). Taken together, we conclude that all three *Tgfb* isoforms are upregulated upon lesion formation at 4 weeks but that each isoform is characterized by a specific expression profile over time and cell type specificity.

Acta1 overexpression correlates with nuclear interaction of serum response factor and MKL1

The upregulation of *Acta1* in the absence of increased *Tgfb* at 2 weeks indicates that *Tgfb*-independent mechanisms of *Acta1* gene
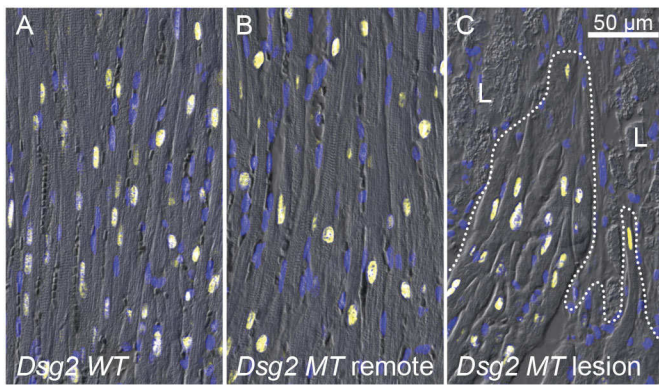
Fig. 5. SRF localizes to nuclei of wild-type and *Dsg2^{mt/mt}* cardiomyocytes. The pictures show representative overlays of differential interference contrast images. Nuclei are stained with DAPI (blue). Anti-SRF immunoreactivity is shown in yellow. (A) Wild-type (*Dsg2 WT*) myocardium, (B) a region far away from lesions (remote) of *Dsg2^{mt/mt}* (*Dsg2 MT*) myocardium and (C) myocardium adjacent to a lesion (L, dotted lines) in a 12-week-old *Dsg2^{mt/mt}* mouse. Myocardium of 2- to 13-week-old mice was stained (wild type, *n*=6; mutant, *n*=8). Scale bar, 50 µm.

regulation must be active at that time. An attractive possibility is mechanical stress-induced upregulation of *Acta1* transcription because of the compromised adhesion between *Dsg2* mutant cardiomyocytes (Kant et al., 2015; Schlipp et al., 2014). It has been proposed that mechanical stress induces nuclear translocation of the cytoplasmic transcriptional co-activator MKL1 in fibroblasts. An increase of F-actin leads to a release of G-actin-bound MKL1 into the cytoplasm. MKL1 subsequently translocates to the nucleus, where it binds to and activates serum response factor

(SRF)-dependent gene transcription (Small, 2012). We therefore wanted to assess whether a similar pathway is activated in fibroblasts and/or cardiomyocytes of *Dsg2*-mutant hearts.

We first examined SRF protein expression in the heart by immunofluorescence microscopy (Fig. 5). In wild-type myocardium, the main immunoreactivity was detectable in the nuclei of cardiomyocytes with only a little labeling of other cell types. A similar staining pattern was observed in *Dsg2^{mt/mt}* myocardium irrespective of disease stage and presence or absence of myocardial lesions (Fig. 5B,C). Immunohistochemistry with two different antibodies against MKL1, however, showed faint signals that were not restricted to the nucleus. To detect specific interaction between SRF and MKL1 in the nucleus, proximity ligation assays (PLA) were carried out (Fig. 6). In wild-type myocardium, the PLA signal was weak and only few cells with nuclear labeling were detected (Fig. 6A,C,G,I,K). In contrast, strong signals were observed in nuclei of cardiomyocytes in 2–4-week-old *Dsg2^{mt/mt}* and *Dsg2^{cKO/cKO}* mice (Fig. 6B,H) even in the absence of myocardial lesions (Fig. 6E). The signal persisted in older mice (Fig. 6D,J,L) with highest number of PLA-positive nuclei in perilesional regions (Fig. 6F). We therefore conclude that activation of SRF through MKL1 translocation to the nucleus mediates *Acta1* gene transcription in *Dsg2^{mt/mt}* and *Dsg2^{cKO/cKO}* hearts prior to and after lesion formation.

ACTA1 overexpression is induced by MKL1 in cultured cardiomyocytes

To test whether nuclear translocation of MKL1 contributes to SRF-dependent *Acta1* gene transcription in cardiomyocytes, HL-1 cardiomyocytes were transfected with a cDNA encoding GFP-tagged MKL1 containing a nuclear localization sequence. The fusion protein was enriched in the nucleus (Fig. 7A) and
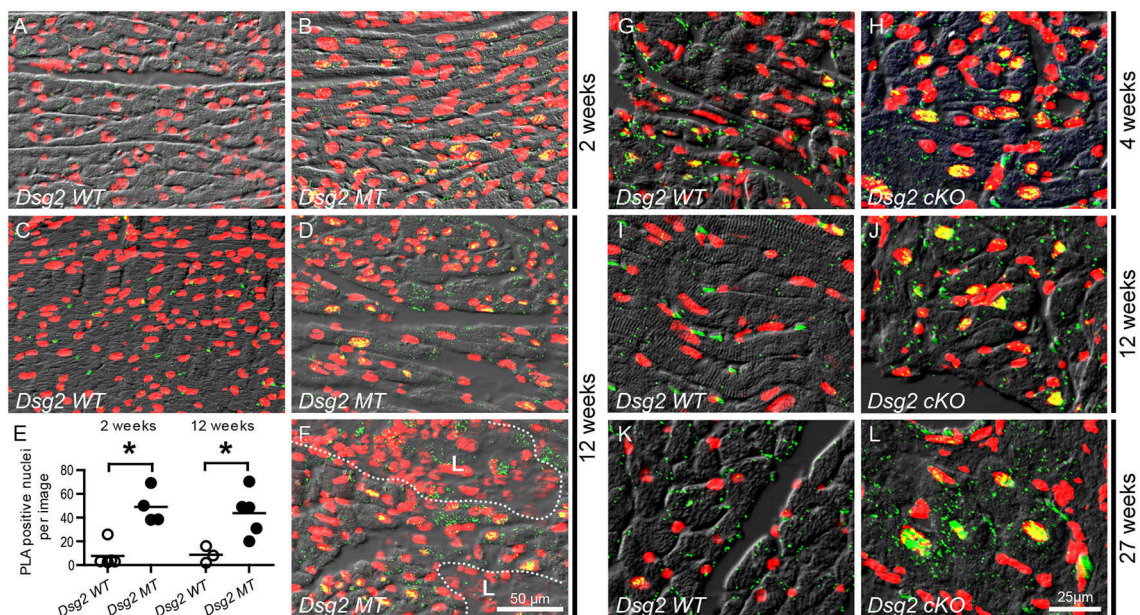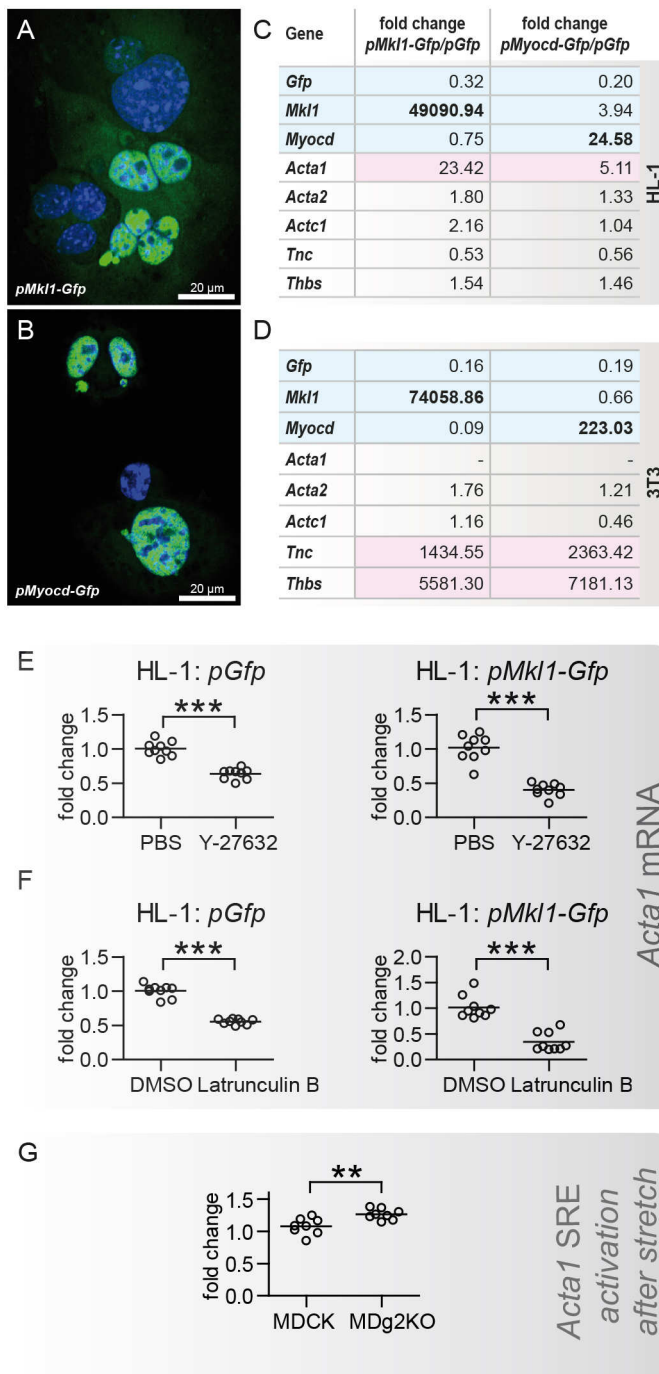

Fig. 6. SRF and MKL1 colocalize in nuclei of *Dsg2^{mt/mt}* and *Dsg2^{cKO/cKO}* cardiomyocytes. (A–D,F–L) The pictures show overlays of differential interference contrast recordings, DAPI staining (false red color) and proximity ligation assay (PLA) signals detecting SRF–MKL1 interaction (green dots, which become yellow when located in the nucleus) in murine hearts. Shown are comparisons of wild type (*Dsg2 WT*) and *Dsg2^{mt/mt}* (*Dsg2 MT*) animals at 2 weeks (A,B; *n*=5 for wild type and *n*=4 for lesion-free mutants) and 12 weeks [C,D,F; *n*=3 for wild type and *n*=5 for the depiction of areas without lesion in mutants in D and with lesions (L; dotted lines) in F] and comparisons of wild-type and *Dsg2^{cKO/cKO}* (*Dsg2 cKO*) at 4 weeks (G,H; *n*=8 for wild type and mutant), 12 weeks (I,J; *n*=8 for wild type and mutant) and at 27 weeks (K,L; *n*=8 for wild type and mutant). Note the highly increased PLA signals in the mutant myocardium at early and late time points and in the presence or absence of myocardial lesions. Scale bars: 50 µm in F (same magnification in A–D); 25 µm in L (same magnifications in G–K). (E) Dot plots showing a comparison of PLA signals in nuclei of wild-type and *Dsg2^{mt/mt}* (*Dsg2 MT*) cardiomyocytes. *P*-values (0.0159 for 2-week-old mice and 0.0357 for 12-week-old mice) were calculated using a Mann–Whitney test. **P*≤0.05.

Fig. 7. *Acta1* transcription is regulated by SRF activation involving MKL1, MYOCD, actin polymerization and DSG2 in cultured cells. (A,B) Fluorescence microscopy of cultured murine HL-1 cardiomyocytes that had been transfected with expression vectors coding for GFP-tagged SRF co-activators MKL1 (*pMkl1-Gfp* in A) or MYOCD (*pMyocd-Gfp* in B). Note the nuclear accumulation of both the GFP-tagged proteins coded by the vector constructs (nuclear counterstain DAPI, blue). Scale bars: 20 μm. (C,D) The tables list relative mRNA expression levels in HL-1 cells (C) and 3T3 fibroblasts (D) that were transfected with either *pMkl1-Gfp* or *pMyocd-Gfp*. HL-1 or 3T3 cells that had been transfected with an expression construct encoding GFP alone (*pGfp*) served as controls. For each transfection, three individual experiments were performed. Note the expected increase of either *Mkl1* or *Myocd* mRNA expression upon transfection with the respective plasmids and the selective upregulation of *Acta1* in HL-1 cardiomyocytes and of *Tnc* and *Thbs* in 3T3 fibroblasts. Housekeeping controls: *Hmbs* and *Hprt*. (E,F) qRT-PCR determination of *Acta1* in *pGfp* transfected or MKL1–GFP-overexpressing HL-1 cells that were treated either with the ROCK inhibitor Y-27632 (660 μM, 24 h) or with latrunculin B (2 μM, 24 h) reveals a reduction in both instances that is not detected in solvent-treated control cells (PBS or DMSO). Housekeeping control: *Hprt*; $P<0.0001$ for all experiments. (G) The plot shows the results of luciferase promoter assays detecting the activity change (fold change) of the major *Acta1* serum response element (SRE) after uniaxial cyclic stretch (20%, 200 mHz, 24 h) in wild-type MDCK and DSG2-depleted MDg2KO cells. SRE activity was determined in eight separate experiments for each genotype with three technical replicas in each experiment. It is significantly increased in MDg2KO cells ($P=0.004$). **$P\leq0.01$; ***$P\leq0.001$.

in HL-1 cells and increased *Tnc* and *Thbs* levels in 3T3 cells, much like MKL1 (Fig. 7C,D).

Increasing G-actin and inhibiting Rho signaling both reduce *Acta1* mRNA in cultured cardiomyocytes

Since MKL1 is sequestered by G-actin in the cytoplasm (cf. Small, 2012), we used latrunculin B to increase G-actin levels in HL-1 cells and monitored changes in *Acta1* mRNA production. qRT-PCR analyses revealed a significant *Acta1* reduction in HL-1 cells that had been either mock-transfected with a vector control encoding GFP or with a GFP-tagged MKL1 expression construct (Fig. 7F).

Rho signaling has also been implicated in upstream regulation of MKL1 transcriptional activation (cf. Small, 2012). We therefore treated HL-1 cells with Y-27632, an inhibitor of the Rho-associated protein kinases (ROCK1 and ROCK2). A 24 h treatment resulted in significant reduction of *Acta1* in both mock-transfected and MKL1-overexpressing HL-1 cells (Fig. 7E).

Depletion of DSG2 leads to increased SRF-dependent *Acta1* promoter activation in mechanically stressed cultured cells

To work out the link between loss of DSG2 and SRF signaling, we decided to use epithelial MDCK cells, which have been useful in desmosome research for many decades (Holthöfer et al., 2007). With the help of CRISPR/Cas9, the *Dsg2* gene was successfully inactivated. The derived clonal cell line MDg2KO was completely devoid of DSG2 as judged by immunofluorescence and immunoblotting (Fig. S6A,B). Similar to the mutant hearts, the amount of desmoplakin was not altered in immunoblots and still localized to desmosome-like puncta at cell borders in immunofluorescence micrographs (Fig. S6A,B). Next, luciferase promoter assays were performed to assess SRF activation. To this end, the 7TFP-SRE reporter construct containing the most-active serum response element of the *Acta1* gene (Parker et al., 1992) was used. The luciferase assays did not reveal significant differences between wild-type MDCK and MDg2KO cells although luciferase activity could be increased by TGFβ and reduced by Y-27632 treatment (Fig. S7). Given the observation that desmosomal proteins

induced a 23-fold upregulation of *Acta1* (Fig. 7C). In contrast, the transcription of other genes containing SRF-binding serum response elements (SREs) such as *Acta2*, *Actc1*, tenascin C (*Tnc*) and thrombospondin 1 (*Thbs1*) were barely affected (Fig. 7C). When 3T3 fibroblasts were transfected with the same construct, however, a different effect on gene expression was observed (Fig. 7D). *Acta1* mRNA remained below the detection limit, while *Tnc* and *Thbs* mRNA expression was strongly increased.

Since it is known that MYOCD, which is an alternative co-activator of SRF, is expressed in cardiomyocytes (Huang et al., 2012), we examined the effects of its nuclear overexpression in cultured cells (Fig. 7B). It induced a 5-fold increase in *Acta1* mRNA

react to increased mechanical loads (Baddam et al., 2018; Price et al., 2018), cells were placed on elastic substrates and subjected to mechanical stress in a cell stretcher. Only intense stimulation (cyclic uniaxial stretching by 20% at 200 mHz for 24 h), which did not visibly alter cell morphology (Fig. S8), led to a significantly increased luciferase expression in MDg2KO cells (Fig. 7G).

DISCUSSION

Increased *Acta1* expression has been described as a common compensatory reaction in stressed myocardium such as occurs in mammalian cardiomyopathies (e.g. Ausma et al., 2001; Clement et al., 1999; Driesen et al., 2009; Schiaffino et al., 1989; Schwartz et al., 1986; Stilli et al., 2006; Suurmeijer et al., 2003). In support of this, biomechanical stretching of cultured cardiomyocytes has been shown to increase *Acta1* expression (Frank et al., 2008). It has been suggested that ACTA1 contributes to increased contractility in the stressed heart. Thus, BALB/c mice with elevated ectopic *Acta1* expression in the heart present increased contractility (Hewett et al., 1994). In accordance, *Acta1* depletion in skeletal muscle is not fully compensated for by *Actc1* gene replacement (Crawford et al., 2002). We therefore propose that the elevated *Acta1* expression in our genetic AC mouse model reflects a compensatory reaction to the mutation-induced desmosomal dysfunction (Hariharan et al., 2014; Kant et al., 2015; Schlipp et al., 2014). The desmosomal adhesion deficiency manifests at the age of 2 weeks when the physiological cardiac workload increases because of accelerated animal growth and thereby imposes increased mechanical stress on the heart (Zhou et al., 2003).

In trying to link increased *Acta1* expression and dysfunctional desmosomal adhesion, we performed analyses based on experimental observations in mechanically stressed fibroblasts (Kuwahara et al., 2005; McGee et al., 2011; Small, 2012) and primary rat cardiomyocytes (Kuwahara et al., 2010). Small proposed for fibroblasts (Small, 2012), that mechanical stress acts through Rho GTPases to release MKL1 from G-actin. MKL1 is then translocated to the nucleus to activate SRF-dependent gene transcription. In analogy, it was found that compromised desmoglein function correlates with increased Rho signaling and elevated F-actin in skin (Waschke et al., 2006). In the current study, we now show increased interaction of SRF and MKL1 in *Dsg2*-mutant hearts. In light of the known upregulation of *Acta1* by SRF (Parker et al., 1992), this finding strongly argues for a MKL1–SRF-dependent elevation of *Acta1* expression in *Dsg2* mutant hearts. This notion is further strengthened by the cell type-specific induction of *Acta1* expression through nuclear overexpression of MKL1 in HL-1 cardiomyocytes. This is further supported by the observation that increasing G-actin, which is known to sequester MKL1 in the cytoplasm, reduces *Acta1* expression. In agreement, *Acta1* activation is mitigated in the stressed myocardium of MKL1-knockout mice (Kuwahara et al., 2010). Furthermore, mechanosensitive MKL1-SRF signaling has been shown to be relevant for actin dynamics in laminopathy (Ho et al., 2013). Moreover, the present study provides evidence for MKL1–SRF-dependent *Acta1* gene transcription in stressed cardiomyocytes within a native tissue context. We suggest that mechanically induced activation of SRF-dependent gene transcription is relevant not only for AC but also for other heart diseases.

When the compensatory capacity of *Dsg2* mutant cardiomyocytes is exhausted, cardiomyocytes become necrotic and are gradually replaced by scar tissue (Kant et al., 2012). Upon scar formation, *Acta1* expression is further elevated (Fig. 1A). Since it has been shown that TGFβ upregulates *Acta1* transcription (MacLellan et al., 1994; Parker et al., 1990), our observation of elevated *Tgfb1* and

Tgfb3 levels in fibrotic lesions and of *Tgfb2* in perilesional cardiomyocytes provides a plausible explanation for this further increase of *Acta1*. Furthermore, mutations in the promoter of the *Tgfb3* gene that presumably increase *Tgfb3* gene transcription have been identified in AC patients (Beffagna et al., 2005).

The local action of TGFβ was reflected by drastically increased *Acta1* mRNA as detected by *in situ* hybridization and by pathological, hitherto unknown, F-actin accumulations at intercalated discs near myocardial lesions in our AC models. The increase in F-actin may further release G-actin-bound MKL1 to stimulate SRF-dependent transcription in a self-amplifying cycle resulting in even higher *Acta1* levels. In addition, TGFB2 produced by stressed cardiomyocytes may enhance this autocrine loop. It will be interesting to find out whether the accumulation of actin at intercalated discs precedes myofibrillar growth, which has been shown to occur in the transitional junction (Bennett et al., 2006; Wilson et al., 2014) and is coupled to transiently increased *Acta1* expression during embryogenesis (Clement et al., 2007). It may be part of the hypertrophic response, which has been described to occur during the chronic disease stage in murine AC models and the human disease (Gerçek et al., 2017).

An unexpected conclusion from our observations is that both pathological stimuli, namely compromised desmosomal adhesion resulting in increased mechanical stress and release of TGFβ by newly-formed lesions, act on SRF-dependent gene transcription through inducing nuclear translocation of MKL1 via a pathway that likely involves RhoA signaling in both instances. Support for this idea comes from our *in vitro* experiments on HL-1 cardiomyocytes (see also Godsel et al., 2010; Small et al., 2010). Interestingly, interference with RhoA signaling is beneficial for patients with heart disease (Shi and Wei, 2013). The relevance of RhoA signaling for cardiomyopathy has also been examined in murine models of cardiac disease. Thus, RhoA overexpression led to dilated cardiomyopathy and increased cardiac fibrosis (Sah et al., 1999). In addition, it has been proposed that RhoA signaling controls hypertrophy, contractility and fibrosis in the myocardium, thereby providing protection against stress-induced heart failure but also facilitating fibrosis (Lauriol et al., 2014). Of note, cardioprotective effects have also been noted in mice, in which the RhoA downstream effectors ROCK1 or ROCK2 were inactivated (Hamid et al., 2007; Okamoto et al., 2013; Zhang et al., 2006).

Conclusions

Fig. 8 graphically summarizes our main findings and puts them in context, placing the cardiomyocyte center stage. We propose that several mechanisms act at different length and time scales during the different stages of pathogenesis in the two *Dsg2*-mutant mouse strains, as below.

Induction of *Acta1* expression prior to lesion formation – 2 weeks

This increase appears to be TGFβ independent (Fig. 4B,E). It likely reflects the overall vulnerability of *Dsg2*-deficient cardiomyocytes to mechanical stress due to adhesion deficiency and is presumably associated with global changes in *Acta1* expression throughout the myocardium (Fig. 1B,D). We propose a mechanical stress-induced mechanism during this disease stage as suggested by observations in mechanically stressed DSG2-depleted MDCK cells (Fig. 7G). It is likely mediated by MKL1 as evidenced by nuclear co-localization of MKL-1 and SRF (Fig. 6B,H).

Induction of *Acta1* expression upon lesion formation – 4–8 weeks

In this situation, an additional TGFβ-dependent mechanism kicks in, which is reflected by an increase in mRNA expression of all three
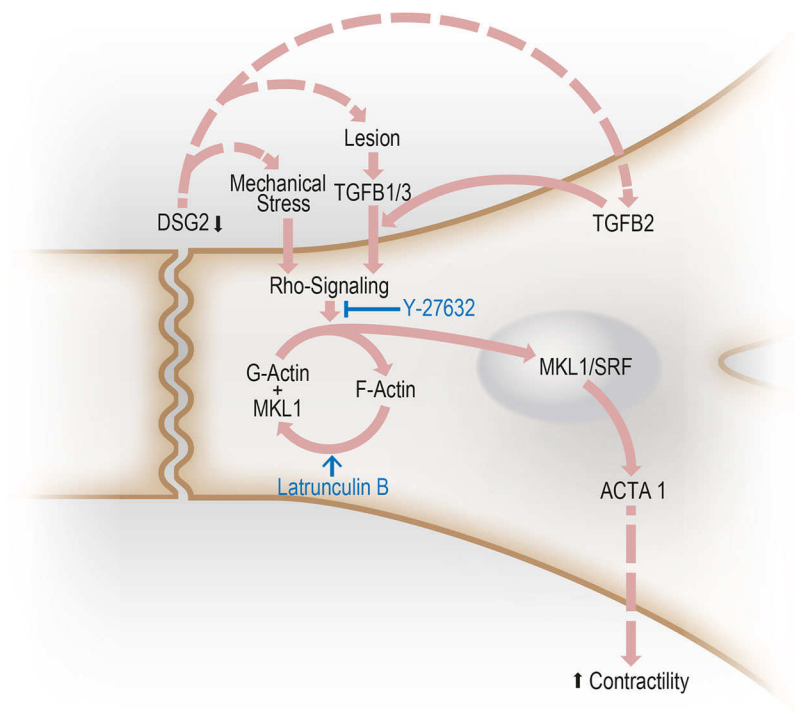
Fig. 8. The schematic summary of our findings depicts how DSG2 mutation leads to increased *Acta1* mRNA that may contribute to increased contractility. *Dsg2* mutation leads to loss of cardiomyocyte adhesion, which results in increased mechanical vulnerability leading to TGFβ-independent mechanical stress-induced signaling during early disease stages and TGFβ-dependent pathway activation upon lesion formation during later disease stages implicating lesional mesenchymal cells, which produce *Tgfb1* and *Tgfb3*, and stressed cardiomyocytes, which produce *Tgfb2*. All may affect Rho signaling, which regulates the equilibrium between F- and G-actin. This notion is supported by inhibitor experiments using Y-27632 to interfere with Rho signaling, and latrunculin B to depolymerize F-actin. A shift to F-actin releases MKL1, which shuttles to the nucleus to activate SRF-dependent *Acta1* gene transcription.

Tgfb isoforms (Fig. 4). It is localized, since increased *Tgfb1* and *Tgfb3* mRNA expression is restricted to fibrosing lesions (Fig. 4A,D). In addition, increased *Tgfb2* mRNA is detected in cardiomyocytes, many of which appear to be damaged and in close vicinity to lesions (Fig. 4C). Based on the known capacity of TGFβ to induce *Acta1* mRNA expression in the myocardium (MacLellan et al., 1994; Parker et al., 1990, 1992), we propose that the increase in TGFβ contributes to the increase in *Acta1* mRNA during this phase of pathogenesis (Fig. 1A,C) and, most importantly, explains the perilesional increase of *Acta1* mRNA (Fig. 1B,D), which leads to conspicuous actin accumulations at intercalated discs with coincident changes in intercalated disc structure later on (Fig. 2C–C″, Fig. 3D–D″; Fig. S1B–B″,D–D″, Fig. S2C–C″). These effects may also be partially mediated by an MKL1- and SRF-dependent mechanism.

Enhanced elevation of Acta1 expression during chronic disease stage – after 8 weeks

This part of the disease process is characterized by a further increase in *Acta1* mRNA (Fig. 1A,C). Mechanical stress may exacerbate compromised desmosomal adhesion, through altering mechanical stimuli provided by fibrotic stiffening of cardiac tissue, which may be responsible for the persistent TGFβ production in fibrotic foci and surrounding cardiomyocytes.

Our observations suggest that the different pathways share a common final path involving Rho signaling, which shifts the equilibrium between G- and F-actin towards F-actin, thereby releasing MKL1. The released MKL1 subsequently shuttles to the nucleus, where it cooperates with SRF to induce *Acta1* gene transcription.

MATERIALS AND METHODS
Animals

The animal experiments were conducted in accordance with the guidelines for the care and use of laboratory animals and approved by the Landesamt für Natur, Umwelt- und Verbraucherschutz Nordrhein-Westfalen (LANUV;

reference number 8.87-50.10.37.09.114). Mice were housed in the animal facility of the Uniklinik RWTH Aachen University. The mouse strains used for all animal experiments are described in Krusche et al. (2011) and Kant et al. (2015).

Heart sample processing

To isolate total RNA from murine hearts, freshly harvested tissue was minced in peqGOLD Lysis-Buffer (Peqlab) using a Dounce homogenizer. Tissue homogenates were stored at −80°C until further processing. Proteins were removed by phenol/chloroform precipitation and total RNA was isolated with the peqGOLD Total RNA kit (Peqlab). DNA contaminations were removed by an on-column DNase digestion step using the peqGOLD DNase I Digest kit (Peqlab).

For fluorescence staining, fresh heart tissue was either snap-frozen in liquid nitrogen or fixed with 4% (w/v) formaldehyde in PBS for 12 h and subsequently embedded in paraffin.

Transcriptome analysis

The quality of the isolated total RNA was assessed by determining the RNA integrity number (RIN factor) using an Agilent 2100 bioanalyzer (Agilent Technologies). GeneChip WT cDNA Synthesis and Amplification, GeneChip WT Terminal Labeling and GeneChip Sample Cleanup Module kits (all from Affymetrix) were employed to prepare labeled cDNA for hybridization with a GeneChip Mouse Gene 1.0 ST (Affymetrix) using a GeneChip Fluidics Station 450 (Affymetrix). Hybridization signals were quantified with a GeneChip Scanner 3000 7G and analyzed with the help of Affymetrix Expression Console software.

qRT-PCR

To prepare cDNA for qRT-PCR, mRNA was reverse-transcribed using the Transcriptor First Strand cDNA Synthesis kit with oligo-(dT)18 oligonucleotides (Roche). qRT-PCR was performed with a LightCycler 96 (Roche), FastStart Essential DNA Probes Master Kit (Roche) and the following primer pairs and UPL-probes (Roche): *Acta1* (10-39 forward, 5′-TCCTCCCTGGAGAAGAGCTA-3′; 10-40 reverse, 5′-ATCCCCGCA-GACTCCATAC-3′; UPL-probe 9), *Acta2* (12-74 forward, 5′-CCAGCACC-ATGAAGATCAAG-3′; 12-75 reverse, 5′-TGGAAGGTAGACAGCGAA GC-3′; UPL-probe 58), *Actb* (12-72 forward, 5′-CTAAGGCCAACCGTG-AAAAG-3′; 12-73 reverse, 5′-ACCAGAGGCATACAGGGACA-3′; UPL-

probe 64), *Actc1* (09-54 forward, 5′-GGAGAAGAGCTATGAACTTCCT-GA-3′; 09-55 reverse, 5′-GCCAGCAGATTCCATACCA-3′; UPL-probe 9), *Actg1* (12-63 forward, 5′-GGAGAGCACGCTGTAGATGA-3′; 12-64 reverse, 5′-CTGTTGGTTAATACCCTGCACA-3′; UPL-probe 64), *Actg2* (12-76 forward, 5′-CCAGCACCATGAAGATCAAG-3′; 12-77 reverse, 5′-ACATTTGCTGGAAGGTGGAG-3′; UPL-probe 58), *Tgfb1* (12-28 forward, 5′-TGGAGCAACATGTGGAACTC-3′; 12-29 reverse, 5′-CAGCAGCCG-GTTACCAAG-3′; UPL-probe 72), *Tgfb2* (13-74 forward, 5′-TCTTC-CGCTTGCAAAACC-3′; 13-75 reverse 5′-GTGGGAGATGTTAAGTCT-TTGGA-3′; UPL-probe 106), *Tgfb3* (13-76 forward, 5′-GCAGACACAA-CCCATAGCAC-3′; 13-77 reverse, 5′-GGGTTCTGCCCACATAGTACA-3′; UPL-probe 1), *Gfp* (15-62 forward, 5′-GAAGCGCGATCACATGGT-3′; 15-63 reverse, 5′-CCATGCCGAGAGTGATCC-3′; UPL-probe 67), *Mkl1* (15-58 forward, 5′-GGCTATGAGGAAGCCATGAG-3′; 15-59 reverse, 5′-GCTCCTTGAAATCTGCTGAAAT-3′; UPL-probe 18), *Myocd* (15-116 forward, 5′-AGAACCATGGGGTCTCTTCA-3′; 15-117 reverse, 5′-CTTG-GGTGCCAGAGAAAGG-3′; UPL-probe 75), *Tnc* (12-30 forward, 5′-ATCTCCTACACAGGGGAGAGAGT-3′; 12-31 reverse, 5′-AAAGATAC-TCAGGATGTACTCTGTGG-3′; UPL-probe 85), *Thbs* (12-22 forward, 5′-GACAAGATCCCCGATGACAG-3′; 12-23 reverse, 5′-GTCTGCTTGG-TCAGGGTTGT-3′; UPL-probe 26), *Hmbs* housekeeping gene (12-36 forward, 5′-AAGTTCCCCCACCTGGAA-3′; 12-37 reverse, 5′-GACGAT-GGCACTGAATTCCT-3′; UPL-probe 42), *Hprt* housekeeping gene (12-65 forward, 5′-TGATAGATCCATTCCTATGACTGTAGA-3′; 12-66 reverse, 5′-AAGACATTCTTTCCAGTTAAAGTTGAG-3′; UPL-probe 22), and *Tbp* housekeeping gene (11-25 forward, 5′-GGGGAGCTGTGATG-TGAAGT-3′; 11-26 reverse, 5′-CCAGGAAATAATTCTGGCTCA-3′; UPL-probe 97).

In situ hybridization
In situ hybridization to detect *Tgfb1*, *Tgfb2*, *Tgfb3*, *Acta1* and *Actc1* mRNA was performed with 1-plex ViewRNA ISH Tissue Assay (QVT0050 and QVT0200; Panomics). 5-μm-thick sections of formaldehyde-fixed, paraffin-embedded heart tissue were processed according to the manufacturer's instructions. The pretreatment to gain access to the tissue mRNA was 20 min protease incubation and 10 min heating at 94–98°C in pretreatment solution. The following Type 1 ViewRNA Probesets from Panomics were used: *Tgfb1* (VB1-14183-01), *Tgfb2* (VB1-16193-01), *Tgfb3* (VB1-16194-01), *Acta1* (VB1-13264-01), *Actc1* (VB1-13263-01). Fluorescence micrographs were recorded with an Apotome.2 microscope setup (Zeiss).

Fluorescence microscopy and proximity ligation assay
To perform immunostainings, 5-μm-thick sections of paraffin-embedded cardiac tissue were incubated in xylene to remove the paraffin (2×10 min) and rehydrated in a graded alcohol series. For immunofluorescence staining of actin, sections were heated in citrate buffer (pH 6.0) in a pressure cooker for 3 min. Afterwards, the primary antibody [diluted in PBS/1.5% bovine serum albumin (BSA)] was applied overnight at 4°C. Primary antibodies were mouse anti-cardiac actin (1:50; 61075, lot: 508010A, Progen), rabbit anti-skeletal muscle actin (1:25; SAB4502543, lot: 310121, Sigma-Aldrich), rabbit anti-desmoglein 2 (1:500; Dsg2 immunohistochemistry is shown in Schlegel et al., 2010) and guinea pig-anti desmoplakin (1:1000; DP-1, lot: 308221, Progen). To stain for SRF, sections were boiled for 10 min in 10 mM Tris(hydroxymethyl)-aminomethan (Tris)-buffer (pH 9.0). Afterwards, rabbit anti-SRF antibodies (1:100 dilution in PBS with 1.5% BSA; sc-335, lot: D3013, Santa Cruz Biotechnology) were applied overnight at 4°C. For phalloidin and cadherin 2 (CDH2) co-staining, cyropreserved heart tissue was cut into 4-μm-thick sections and subsequently fixed in 2% (w/v) formaldehyde in PBS at 4°C for 10 min. Tissue slices were then permeabilized for 30 s with 0.1% Triton X-100 (v/v) in PBS, washed twice with TBST [50 mM Tris-HCl pH 7.5, 0.3 M NaCl; 0.05% (v/v) Tween 20] and incubated with phalloidin–Alexa 488 (1:40; A12379, Life Technologies) and rabbit anti-cadherin 2 antibodies (1:500; ab12221, lot: GR139340-5, Abcam). MDCK and MDg2KO cells were grown on cover-slips for DSG2 and DSP immunostaining. Coverslips were washed in pre-warmed Dulbecco's PBS (Sigma-Aldrich) and cells were fixed for 3 min in precooled methanol (−20°C) followed by a 20 s fixation

step in precooled acetone (−20°C). Afterwards, the primary antibodies (diluted in PBS with 1.5% BSA) were applied for 1 h at room temperature. Primary antibodies were rabbit anti-DSG2 (1:500; Schlegel et al., 2010) and guinea pig anti-DSP (1:1000; DP-1, lot: 308221, Progen).

In all instances, three 5 min washings in modified TBST ensued, and were followed by secondary antibody incubation for 1 h at room temperature [Alexa 488-conjugated goat anti-rabbit (A-11070), goat anti-mouse (A-11029) or Alexa 555 goat anti-guinea pig (A-21435) antibodies, all from Life Technologies and diluted 1:500 in PBS with 1.5% BSA]. Sections were subsequently washed three times in modified TBST. Background reduction for tissue sections was achieved by a 30 min incubation in 0.1% Sudan Black B (Merck) dissolved in 70% ethanol. Again, slides were washed three times in modified TBST and mounted in Mowiol 4-88 (Roth). Fluorescence micrographs were recorded with an Apotome.2 microscope setup.

To perform proximity ligation assays, 5-μm-thick sections of paraffin-embedded tissue were deparaffinized with xylene, rehydrated, boiled for 10 min in 10 mM Tris buffer (pH 9.0) and incubated with the following primary antibodies overnight at 4°C: rabbit anti-SRF antibody (1:100; sc-335, lot: D3013, Santa Cruz Biotechnology) and goat anti-MKL1 antibody (1:25; sc-21558, lot: I1412, Santa Cruz Biotechnology) diluted in PBS with 1.5% BSA. Subsequent proximity ligation assay was carried out with the Duolink In Situ Orange Starter kit Goat/Rabbit (DUO92106, Sigma-Aldrich) following the instructions provided by the manufacturer. Finally, slides were washed three times in modified TBST and mounted in Mowiol 4-88 (Roth). Fluorescence micrographs were recorded with an Apotome.2 microscope. Single pictures were recorded per slide in cases of low signals and up to five pictures were recorded of different areas in cases of strong signals. Afterwards, the PLA signal was overlaid with recordings of nuclear DAPI staining. PLA dots were counted in each nucleus and nuclei with more than four PLA dots were counted as positive. Subsequently, the average of PLA-positive nuclei per image was calculated for each slide and statistics were performed.

Immunoblots
Confluent cell layers from T25 cell culture flasks were directly lysed each in 200 μl SDS sample buffer. After heating to 60°C for 20 min and a short centrifugation step, 20 μl were loaded per lane on 8% SDS-polyacrylamide gels. Proteins were separated by gel electrophoresis and transferred onto polyvinylidene fluoride (PVDF) membranes using tank blotting. Membranes were afterwards blocked with 5% (w/v) low-fat milk powder (Roth) in TBST [50 mM Tris-HCl pH 7.6, 150 mM NaCl, 0.1% (v/v) Tween 20] for 2 h, washed three times for 5 min each with TBST and incubated with primary antibody diluted in TBST with 1% low-fat milk powder overnight at 4°C. Antibody dilutions were: 1:1000 for polyclonal guinea pig anti-DSG2 antibodies (Kant et al., 2015), 1:1500 for guinea pig anti-DSP (DP-1, Progen), and 1:2000 for polyclonal rabbit anti-actin antibodies (A2066, Sigma). Membranes were washed three times in TBST and incubated for 1 h with horseradish peroxidase-coupled secondary antibodies (anti-rabbit IgG and anti-guinea pig IgG antibodies from DAKO at 1:4000 diluted in TBST with 1% low-fat milk powder). Signals were detected using ECL prime (GE healthcare) and a chemiluminescence imaging system (Fusion SL, Vilber Lourmat).

DNA cloning
To clone *pMkl1-Gfp* and *pMyocd-Gfp* the vectors *p3xFLAG-Mkl1* (Cen et al., 2003), tetO-Myocd (Addis et al., 2013) and *pEgfp-N3* (Clontech) were used. All newly prepared plasmids were sequenced to verify correct cloning.

To clone *pMkl1-Gfp*, a CMV promoter-driven mammalian expression vector coding for a GFP-tagged version of murine MKL1, the *Mkl1* cDNA sequence was first amplified from vector *p3xFLAG-Mkl1* (Cen et al., 2003) using oligonucelotides 14-137 (5′-GCTCAAGCTTATGCCGCCTTTGA-AAAGTCC-3′) and 14-138 (5′-GCGTCGACTATGACCTTTCTTTTCT-TTTTTGGCAAGCAGGAATCCCAGT-3′) introducing a nuclear localization signal together with a HindIII and a SalI restriction site at the 5′- and 3′-end, respectively. Then vector *pEgfp-N3* (Clontech) and the PCR product were cut with HindIII and SalI. Purified fragments were ligated to generate *pMkl1-Gfp*. To obtain the control plasmid *pGfp*, a fragment

containing a nuclear localization signal fused to *Gfp* was amplified from *pMkl1-Gfp* by using oligonucleotides 14-155 (5′-GAGCTCAAGCTTAT-GCACTGGGATTCCTGCTTGCCAAA-3′) and 14-156 (5′-TTTCAGGT-TCAGGGGGAGGTGT-3′). The amplicon and pEGFP-N3 (Clontech) were then cut with HindIII and NotI and purified fragments were ligated to form *pGfp*.

To clone *pMyocd-Gfp*, a mammalian expression construct for GFP-tagged MYOCD, the coding sequence of *Myocd* was amplified from plasmid *tetO-Myocd* (Addis et al., 2013) with the help of oligonucleotides 14-143 (5′-GCGAAGCTTATGACACTCCTGGGGTCTGAACACTC-3′) and 14-144 (5′-GGCGTCGACGACCTTTCTTTTCTTTTTTGGCCACT-GCTGTAAGTGGAGATCCATAGGG-3′). The resulting fragment was ligated into *pEgfp-N3* after cleavage with HindIII and SalI. All newly prepared plasmids were sequenced to verify correct cloning.

To clone luciferase reporter construct 7TFP-SRE, plasmic 7TFP [Addgene plasmid #24308, deposited by Roel Nusse (Fuerer and Nusse, 2010)] was cut with PstI and NheI. To introduce the most-efficient serum response element from *Acta1* promotor (SRE1 in Parker et al., 1992) oligonucleotides 17-142 (5′-GCCCGACACCCAAATATGGCGACGGC-CG-3′) and 17-143 (5′-CTAGCGGCCGTCGCCATATTTGGGTGTCGG-GCTGCA-3′) were annealed, phosphorylated using a T4-polynucleotide kinase (New England Biolabs) and ligated to the bigger 7TFP fragment produced beforehand.

To prepare the canine *Dsg2* CRISPR knock-out plasmid sgRNA cDsg2 pSpCas9(BB)-2A-Puro(PX459)V2.0, pSpCas9(BB)-2A-Puro(PX459)V2.0 [Addgene plasmid #62988; deposited by from Feng Zhang (Ran et al., 2013)] was cut with BbsI. The resulting fragment was then ligated to the annealed and T4-polynucleotide kinase phosphorylated oligonucleotides 17-112 (5′-CACCGCGCGATGGCGCGGAGCGCGG-3′) and 17-113 (5′-AAACCCGCGCTCCGCGCCATCGCGC-3′).

Cell culture

Murine atrial HL-1 cardiomyocytes (Claycomb et al., 1998) were grown in cell culture dishes that had been coated with fibronectin [7 µg ml^{-1} (Sigma Aldrich) for 30 min at 37°C]. Claycomb medium (Sigma-Aldrich) supplemented with 10% (v/v) horse serum (Sigma-Aldrich; 12449C), 0.1 mM norepinephrine bitartrate salt (Sigma-Aldrich) and 2 mM L-alanyl-L-glutamine (Glutamax; Gibco) was used. For transfection, 3.0×10^6 cells were electroporated with an AMAXA Nucleofector II device (Lonza) using program A-033, the Cell Line Nucleofector Kit V (Lonza) and 10 µg plasmid DNA. Electroporated cells were subsequently suspended in 1 ml pre-warmed Claycomb medium and seeded in a fibronectin-coated well of a six-well dish.

NIH-3T3 cells were grown in DMEM AQ medium (Sigma-Aldrich) supplemented with 10% (v/v) fetal calf serum GOLD (PAA; A15-151). To transfect NIH-3T3 cells, they were seeded in six-well plates and grown to ~40% confluence. 3 µg plasmid-DNA were used per well to transfect cells with jetPEI (Polyplus Transfection).

At 2 days after transfection of either cell type, cells were harvested for RNA isolation using the RNeasy Mini Kit (Qiagen).

To determine transfection efficiency and localization of transgenic fusion proteins, cells were grown on coverslips prior to transfection. At different time points the coverslips were removed, washed in pre-warmed Dulbecco's PBS (Sigma-Aldrich) and the cells were fixed for 3 min in precooled methanol (−20°C) followed by a 20 s long fixation step in precooled acetone (−20°C). For fluorescence microscopy, coverslips were mounted in Mowiol 4-88 (Roth) containing 2 µg ml^{-1} Hoechst 33342 (Molecular Probes). Fluorescence images were recorded with an Apotome.2 microscope (Zeiss).

To establish Dsg2 knock-out MDCK cell lines, MDCK cells were seeded in six-well plates and grown to ~60% confluence in DMEM AQ medium (Sigma-Aldrich) supplemented with 10% (v/v) fetal calf serum GOLD (PAA; A15-151). 3 µg sgRNA cDsg2 pSpCas9(BB)-2A-Puro(PX459)V2.0 plasmid-DNA were used per well to transfect cells with the help of jetPEI (Polyplus Transfection). At 1 day after transfection cells were treated with 6 µg/ml puromycin (PAA) for 4 weeks. Resulting resistant cell clones were checked for DSG2 knockout by anti-DSG2 immunofluorescence and immunoblotting.

For luciferase reporter assays, MDCK and MDg2KO cells were grown in DMEM AQ medium supplemented with 1% (v/v) fetal calf serum GOLD. Cells were seeded in 6-cm petri dishes and grown to ~60% confluence. 5 µg 7TFP-SRE plasmid-DNA and 1 µg pRL-TK (*Renilla* Luciferase Control Vector for normalization of reporter assays, Promega, E6921) were used per dish to transfect cells with jetPEI (Polyplus Transfection). After another 4 days, cells were processed for SRE promotor activity assays.

All cultured cells were tested for mycoplasma contaminations using a PCR assay.

In some instances, cells were treated with the actin-depolymerizing drug latrunculin B (Adipogen). Latrunculin B was dissolved in DMSO at 10 mM. HL-1 cells at 80–90% confluency were incubated with 2 µM latrunculin B for 24 h prior to further analysis. In other experiments, HL-1 or 7TFP-SRE and pRL-TK transfected MDCK cells were incubated with the Rho-associated protein kinase (ROCK) inhibitor Y-27632 (Stemcell Technologies, dissolved in PBS at 20 mM) for 24 h at 66 µM. To induce SRF signaling 7TFP-SRE and pRL-TK transfected MDCK cells were incubated with recombinant human TGFB1 (Peprotech, dissolved in PBS at 2.5 µg/ml) for 24 h at 2.5 ng/ml.

Elastic substrate preparation and cell stretching

Elastic silicone chambers for stretch experiments were prepared and calibrated as described previously (Faust et al., 2011). Elasticities were set to 50 kPa and chambers were coated with fibronectin (20 µg/ml) in PBS for 1 h at 37°C. Cells were then seeded on the elastomer substrates and incubated overnight. Cells were then cyclically stretched with a cell stretcher for 24 h at 200 mHz and 20% uniaxial stretch (Faust et al., 2011).

SRE promotor activity assays

To perform SRE promotor activity assays 7TFP-SRE and pRL-TK transfected MDCK and MDg2KO cells were washed once with PBS and subsequently lysed in 250 µl passive lysis buffer (Promega). Samples were cleared by a 1 minute centrifugation at 17,000 *g* and three 50 µl technical replicates were examined with the Dual-Luciferase Reporter Assay System (Promega, E1910). A GloMax Navigator Microplate Luminometer (Promega, GM2010) was used for measurements injecting 50 µl of each substrate per replicate and set to an integration time of 10 s. The SRE-specific luciferase signals were normalized to the control *Renilla* signals.

Statistical methods

All results are presented as mean±standard deviation (s.d.). The mean of data gathered from one animal or one independent transfection was counted as *n*=1. Datasets were tested for Gaussian distribution with the D'Agostino and Pearson omnibus normality test. When datasets were not Gaussian distributed, nonparametric statistical tests were used. Statistical analyses comparing two groups with each other were performed with either the two-tailed Mann–Whitney test or the two-tailed *t*-test using 95% confidence intervals. Statistical analyses comparing three groups were accomplished by either the Kruskal–Wallis test together with Dunn's post hoc test or ANOVA analysis followed by the Bonferroni post hoc test using 95% confidence intervals. Statistical analyses for expression over time were calculated using a two-way ANOVA followed by a Bonferroni post hoc test. All statistical analyses were performed with GraphPad Prism5. * indicates results with $P \leq 0.05$, ** indicates $P \leq 0.01$ and *** indicates $P \leq 0.001$.

Author contributions

Conceptualization: S.K., C.A.K., R.E.L.; Methodology: S.K., R.M., B.H., C.A.K.; Validation: B.F., S.K.; Formal analysis: S.K., B.F., A.H., A.R.; Investigation: S.K.,

Supplementary information
Supplementary information available online at
http://jcs.biologists.org/lookup/doi/10.1242/jcs.199612.supplemental

References

Addis, R. C., Ifkovits, J. L., Pinto, F., Kellam, L. D., Esteso, P., Rentschler, S., Christoforou, N., Epstein, J. A. and Gearhart, J. D. (2013). Optimization of direct fibroblast reprogramming to cardiomyocytes using calcium activity as a functional measure of success. *J. Mol. Cell. Cardiol.* **60**, 97-106.

Agullo-Pascual, E., Cerrone, M. and Delmar, M. (2014). Arrhythmogenic cardiomyopathy and Brugada syndrome: diseases of the connexome. *FEBS Lett.* **588**, 1322-1330.

Ausma, J., Litjens, N., Lenders, M.-H., Duimel, H., Mast, F., Wouters, L., Ramaekers, F., Allessie, M. and Borgers, M. (2001). Time course of atrial fibrillation-induced cellular structural remodeling in atria of the goat. *J. Mol. Cell. Cardiol.* **33**, 2083-2094.

Awad, M. M., Dalal, D., Cho, E., Amat-Alarcon, N., James, C., Tichnell, C., Tucker, A., Russell, S. D., Bluemke, D. A., Dietz, H. C. et al. (2006). DSG2 mutations contribute to arrhythmogenic right ventricular dysplasia/ cardiomyopathy. *Am. J. Hum. Genet.* **79**, 136-142.

Baddam, S., Arsenovic, P., Narayanan, V., Duggan, N., Mayer, C., Newman, S., Abutaleb, D., Mohan, A., Kowalczyk, A. and Conway, D. (2018). The desmosomal cadherin desmoglein-2 experiences mechanical tension as demonstrated by a FRET-based tension biosensor expressed in living cells. *Cells* **7**, 66.

Basso, C., Bauce, B., Corrado, D. and Thiene, G. (2011). Pathophysiology of arrhythmogenic cardiomyopathy. *Nat. Rev. Cardiol.* **9**, 223-233.

Bauce, B., Nava, A., Beffagna, G., Basso, C., Lorenzon, A., Smaniotto, G., De Bortoli, M., Rigato, I., Mazzotti, E., Steriotis, A. et al. (2010). Multiple mutations in desmosomal proteins encoding genes in arrhythmogenic right ventricular cardiomyopathy/dysplasia. *Heart Rhythm.* **7**, 22-29.

Beffagna, G., Occhi, G., Nava, A., Vitiello, L., Ditadi, A., Basso, C., Bauce, B., Carraro, G., Thiene, G., Towbin, J. A. et al. (2005). Regulatory mutations in transforming growth factor-beta3 gene cause arrhythmogenic right ventricular cardiomyopathy type 1. *Cardiovasc. Res.* **65**, 366-373.

Bennett, P. M., Maggs, A. M., Baines, A. J. and Pinder, J. C. (2006). The transitional junction: a new functional subcellular domain at the intercalated disc. *Mol. Biol. Cell* **17**, 2091-2100.

Cen, B., Selvaraj, A., Burgess, R. C., Hitzler, J. K., Ma, Z., Morris, S. W. and Prywes, R. (2003). Megakaryoblastic leukemia 1, a potent transcriptional coactivator for serum response factor (SRF), is required for serum induction of SRF target genes. *Mol. Cell. Biol.* **23**, 6597-6608.

Claycomb, W. C., Lanson, N. A., Jr, Stallworth, B. S., Egeland, D. B., Delcarpio, J. B., Bahinski, A. and Izzo, N. J.Jr. (1998). HL-1 cells: a cardiac muscle cell line that contracts and retains phenotypic characteristics of the adult cardiomyocyte. *Proc. Natl. Acad. Sci. USA* **95**, 2979-2984.

Clément, S., Chaponnier, C. and Gabbiani, G. (1999). A subpopulation of cardiomyocytes expressing alpha-skeletal actin is identified by a specific polyclonal antibody. *Circ. Res.* **85**, e51-e58.

Clement, S., Stouffs, M., Bettiol, E., Kampf, S., Krause, K.-H., Chaponnier, C. and Jaconi, M. (2007). Expression and function of alpha-smooth muscle actin during embryonic-stem-cell-derived cardiomyocyte differentiation. *J. Cell Sci.* **120**, 229-238.

Crawford, K., Flick, R., Close, L., Shelly, D., Paul, R., Bove, K., Kumar, A. and Lessard, J. (2002). Mice lacking skeletal muscle actin show reduced muscle strength and growth deficits and die during the neonatal period. *Mol. Cell. Biol.* **22**, 5887-5896.

Delmar, M. and McKenna, W. J. (2010). The cardiac desmosome and arrhythmogenic cardiomyopathies: from gene to disease. *Circ. Res.* **107**, 700-714.

Driesen, R. B., Verheyen, F. K., Debie, W., Blaauw, E., Babiker, F. A., Cornelussen, R. N. M., Ausma, J., Lenders, M.-H., Borgers, M., Chaponnier, C. et al. (2009). Re-expression of alpha skeletal actin as a marker for dedifferentiation in cardiac pathologies. *J. Cell. Mol. Med.* **13**, 896-908.

Faust, U., Hampe, N., Rubner, W., Kirchgessner, N., Safran, S., Hoffmann, B. and Merkel, R. (2011). Cyclic stress at mHz frequencies aligns fibroblasts in direction of zero strain. *PLoS ONE* **6**, e28963.

Frank, D., Kuhn, C., Brors, B., Hanselmann, C., Lüdde, M., Katus, H. A. and Frey, N. (2008). Gene expression pattern in biomechanically stretched cardiomyocytes: evidence for a stretch-specific gene program. *Hypertension* **51**, 309-318.

Franke, W. W., Stehr, S., Stumpp, S., Kuhn, C., Heid, H., Rackwitz, H.-R., Schnolzer, M., Baumann, R., Holzhausen, H.-J. and Moll, R. (1996). Specific immunohistochemical detection of cardiac/fetal alpha-actin in human cardiomyocytes and regenerating skeletal muscle cells. *Differentiation* **60**, 245-250.

Franke, W. W., Borrmann, C. M., Grund, C. and Pieperhoff, S. (2006). The area composita of adhering junctions connecting heart muscle cells of vertebrates. I. Molecular definition in intercalated disks of cardiomyocytes by immunoelectron microscopy of desmosomal proteins. *Eur. J. Cell Biol.* **85**, 69-82.

Fuerer, C. and Nusse, R. (2010). Lentiviral vectors to probe and manipulate the Wnt signaling pathway. *PLoS ONE* **5**, e9370.

Gerçek, M., Gerçek, M., Kant, S., Simsekyilmaz, S., Kassner, A., Milting, H., Liehn, E. A., Leube, R. E. and Krusche, C. A. (2017). Cardiomyocyte hypertrophy in arrhythmogenic cardiomyopathy. *Am. J. Pathol.* **187**, 752-766.

Godsel, L. M., Dubash, A. D., Bass-Zubek, A. E., Amargo, E. V., Klessner, J. L., Hobbs, R. P., Chen, X. and Green, K. J. (2010). Plakophilin 2 couples actomyosin remodeling to desmosomal plaque assembly via RhoA. *Mol. Biol. Cell* **21**, 2844-2859.

Groeneweg, J. A., Bhonsale, A., James, C. A., te Riele, A. S., Dooijes, D., Tichnell, C., Murray, B., Wiesfeld, A. C. P., Sawant, A. C., Kassamali, B. et al. (2015). Clinical presentation, long-term follow-Up, and outcomes of 1001 arrhythmogenic right ventricular dysplasia/cardiomyopathy patients and family members. *Circ. Cardiovasc Genet.* **8**, 437-446.

Hamid, S. A., Bower, H. S. and Baxter, G. F. (2007). Rho kinase activation plays a major role as a mediator of irreversible injury in reperfused myocardium. *Am. J. Physiol. Heart Circ. Physiol.* **292**, H2598-H2606.

Hariharan, V., Asimaki, A., Michaelson, J. E., Plovie, E., MacRae, C. A., Saffitz, J. E. and Huang, H. (2014). Arrhythmogenic right ventricular cardiomyopathy mutations alter shear response without changes in cell-cell adhesion. *Cardiovasc. Res.* **104**, 280-289.

Hewett, T. E., Grupp, I. L., Grupp, G. and Robbins, J. (1994). Alpha-skeletal actin is associated with increased contractility in the mouse heart. *Circ. Res.* **74**, 740-746.

Ho, C. Y., Jaalouk, D. E., Vartiainen, M. K. and Lammerding, J. (2013). Lamin A/C and emerin regulate MKL1-SRF activity by modulating actin dynamics. *Nature* **497**, 507-511.

Holthöfer, B., Windoffer, R., Troyanovsky, S. and Leube, R. E. (2007). Structure and function of desmosomes. *Int. Rev. Cytol.* **264**, 65-163.

Hoorntje, E. T., Te Rijdt, W. P., James, C. A., Pilichou, K., Basso, C., Judge, D. P., Bezzina, C. R. and van Tintelen, J. P. (2017). Arrhythmogenic cardiomyopathy: pathology, genetics, and concepts in pathogenesis. *Cardiovasc. Res.* **113**, 1521-1531.

Huang, J., Elicker, J., Bowens, N., Liu, X., Cheng, L., Cappola, T. P., Zhu, X. and Parmacek, M. S. (2012). Myocardin regulates BMP10 expression and is required for heart development. *J. Clin. Invest.* **122**, 3678-3691.

Kant, S., Krull, P., Eisner, S., Leube, R. E. and Krusche, C. A. (2012). Histological and ultrastructural abnormalities in murine desmoglein 2-mutant hearts. *Cell Tissue Res.* **348**, 249-259.

Kant, S., Holthöfer, B., Magin, T. M., Krusche, C. A. and Leube, R. E. (2015). Desmoglein 2-dependent arrhythmogenic cardiomyopathy is caused by a loss of adhesive function. *Circ Cardiovasc Genet.* **8**, 553-563.

Kritzik, M. R., Lago, C. U., Kayali, A. G., Arnaud-Dabernat, S., Liu, G., Zhang, Y.-Q., Hua, H., Fox, H. S. and Sarvetnick, N. E. (2010). Epithelial progenitor 1, a novel factor associated with epithelial cell growth and differentiation. *Endocrine* **37**, 312-321.

Krusche, C. A., Holthöfer, B., Hofe, V., van de Sandt, A. M., Eshkind, L., Bockamp, E., Merx, M. W., Kant, S., Windoffer, R. and Leube, R. E. (2011). Desmoglein 2 mutant mice develop cardiac fibrosis and dilation. *Basic Res. Cardiol.* **106**, 617-633.

Kuwahara, K., Barrientos, T., Pipes, G. C. T., Li, S. and Olson, E. N. (2005). Muscle-specific signaling mechanism that links actin dynamics to serum response factor. *Mol. Cell. Biol.* **25**, 3173-3181.

Kuwahara, K., Kinoshita, H., Kuwabara, Y., Nakagawa, Y., Usami, S., Minami, T., Yamada, Y., Fujiwara, M. and Nakao, K. (2010). Myocardin-related transcription factor A is a common mediator of mechanical stress- and neurohumoral stimulation-induced cardiac hypertrophic signaling leading to activation of brain natriuretic peptide gene expression. *Mol. Cell. Biol.* **30**, 4134-4148.

Lauriol, J., Keith, K., Jaffre, F., Couvillon, A., Saci, A., Goonasekera, S. A., McCarthy, J. R., Kessinger, C. W., Wang, J., Ke, Q. et al. (2014). RhoA signaling in cardiomyocytes protects against stress-induced heart failure but facilitates cardiac fibrosis. *Sci. Signal.* **7**, ra100.

Lodder, E. M. and Rizzo, S. (2012). Mouse models in arrhythmogenic right ventricular cardiomyopathy. *Front. Physiol.* **3**, 221.

MacLellan, W. R., Lee, T. C., Schwartz, R. J. and Schneider, M. D. (1994). Transforming growth factor-beta response elements of the skeletal alpha-actin gene. Combinatorial action of serum response factor, YY1, and the SV40 enhancer-binding protein, TEF-1. *J. Biol. Chem.* **269**, 16754-16760.

McGee, K. M., Vartiainen, M. K., Khaw, P. T., Treisman, R. and Bailly, M. (2011). Nuclear transport of the serum response factor coactivator MRTF-A is downregulated at tensional homeostasis. *EMBO Rep.* **12**, 963-970.

Moll, R., Holzhausen, H.-J., Mennel, H.-D., Kuhn, C., Baumann, R., Taege, C. and Franke, W. W. (2006). The cardiac isoform of alpha-actin in regenerating and atrophic skeletal muscle, myopathies and rhabdomyomatous tumors: an immunohistochemical study using monoclonal antibodies. *Virchows Arch.* **449**, 175-191.

Nekrasova, O. and Green, K. J. (2013). Desmosome assembly and dynamics. *Trends Cell Biol.* **23**, 537-546.

Okamoto, R., Li, Y., Noma, K., Hiroi, Y., Liu, P.-Y., Taniguchi, M., Ito, M. and Liao, J. K. (2013). FHL2 prevents cardiac hypertrophy in mice with cardiac-specific deletion of ROCK2. *FASEB J.* **27**, 1439-1449.

Parker, T. G., Chow, K. L., Schwartz, R. J. and Schneider, M. D. (1990). Differential regulation of skeletal alpha-actin transcription in cardiac muscle by two rfibroblast growth factors. *Proc. Natl. Acad. Sci. USA* **87**, 7066-7070.

Parker, T. G., Chow, K. L., Schwartz, R. J. and Schneider, M. D. (1992). Positive and negative control of the skeletal alpha-actin promoter in cardiac muscle. A proximal serum response element is sufficient for induction by basic fibroblast growth factor (FGF) but not for inhibition by acidic FGF. *J. Biol. Chem.* **267**, 3343-3350.

Pilichou, K., Nava, A., Basso, C., Beffagna, G., Bauce, B., Lorenzon, A., Frigo, G., Vettori, A., Valente, M., Towbin, J. et al. (2006). Mutations in desmoglein-2 gene are associated with arrhythmogenic right ventricular cardiomyopathy. *Circulation* **113**, 1171-1179.

Pilichou, K., Remme, C. A., Basso, C., Campian, M. E., Rizzo, S., Barnett, P., Scicluna, B. P., Bauce, B., van den Hoff, M. J. B., de Bakker, J. M. T. et al. (2009). Myocyte necrosis underlies progressive myocardial dystrophy in mouse dsg2-related arrhythmogenic right ventricular cardiomyopathy. *J. Exp. Med.* **206**, 1787-1802.

Price, A. J., Cost, A.-L., Ungewiss, H., Waschke, J., Dunn, A. R. and Grashoff, C. (2018). Mechanical loading of desmosomes depends on the magnitude and orientation of external stress. *Nat. Commun.* **9**, 5284.

Ran, F. A., Hsu, P. D., Wright, J., Agarwala, V., Scott, D. A. and Zhang, F. (2013). Genome engineering using the CRISPR-Cas9 system. *Nat. Protoc.* **8**, 2281-2308.

Rickelt, S. and Pieperhoff, S. (2012). Mutations with pathogenic potential in proteins located in or at the composite junctions of the intercalated disk connecting mammalian cardiomyocytes: a reference thesaurus for arrhythmogenic cardiomyopathies and for Naxos and Carvajal diseases. *Cell Tissue Res.* **348**, 325-333.

Sah, V. P., Minamisawa, S., Tam, S. P., Wu, T. H., Dorn, G. W., II, Ross, J., Jr, Chien, K. R. and Brown, J. H. (1999). Cardiac-specific overexpression of RhoA results in sinus and atrioventricular nodal dysfunction and contractile failure. *J. Clin. Invest.* **103**, 1627-1634.

Schiaffino, S., Samuel, J. L., Sassoon, D., Lompré, A. M., Garner, I., Marotte, F., Buckingham, M., Rappaport, L. and Schwartz, K. (1989). Nonsynchronous accumulation of alpha-skeletal actin and beta-myosin heavy chain mRNAs during early stages of pressure-overload–induced cardiac hypertrophy demonstrated by in situ hybridization. *Circ. Res.* **64**, 937-948.

Schlegel, N., Meir, M., Heupel, W.-M., Holthöfer, B., Leube, R. E. and Waschke, J. (2010). Desmoglein 2-mediated adhesion is required for intestinal epithelial barrier integrity. *Am. J. Physiol. Gastrointest. Liver Physiol.* **298**, G774-G783.

Schlipp, A., Schinner, C., Spindler, V., Vielmuth, F., Gehmlich, K., Syrris, P., McKenna, W. J., Dendorfer, A., Hartlieb, E. and Waschke, J. (2014). Desmoglein-2 interaction is crucial for cardiomyocyte cohesion and function. *Cardiovasc. Res.* **104**, 245-257.

Schwartz, K., de la Bastie, D., Bouveret, P., Oliviéro, P., Alonso, S. and Buckingham, M. (1986). Alpha-skeletal muscle actin mRNA's accumulate in hypertrophied adult rat hearts. *Circ. Res.* **59**, 551-555.

Shi, J. and Wei, L. (2013). Rho kinases in cardiovascular physiology and pathophysiology: the effect of fasudil. *J. Cardiovasc. Pharmacol.* **62**, 341-354.

Small, E. M. (2012). The actin-MRTF-SRF gene regulatory axis and myofibroblast differentiation. *J. Cardiovasc. Transl. Res.* **5**, 794-804.

Small, E. M., Thatcher, J. E., Sutherland, L. B., Kinoshita, H., Gerard, R. D., Richardson, J. A., Dimaio, J. M., Sadek, H., Kuwahara, K. and Olson, E. N. (2010). Myocardin-related transcription factor-a controls myofibroblast activation and fibrosis in response to myocardial infarction. *Circ. Res.* **107**, 294-304.

Stilli, D., Bocchi, L., Berni, R., Zaniboni, M., Cacciani, F., Chaponnier, C., Musso, E., Gabbiani, G. and Clément, S. (2006). Correlation of alpha-skeletal actin expression, ventricular fibrosis and heart function with the degree of pressure overload cardiac hypertrophy in rats. *Exp. Physiol.* **91**, 571-580.

Suurmeijer, A. J., Clement, S., Francesconi, A., Bocchi, L., Angelini, A., Van Veldhuisen, D. J., Spagnoli, L. G., Gabbiani, G. and Orlandi, A. (2003). Alpha-actin isoform distribution in normal and failing human heart: a morphological, morphometric, and biochemical study. *J. Pathol.* **199**, 387-397.

Syrris, P., Ward, D., Asimaki, A., Evans, A., Sen-Chowdhry, S., Hughes, S. E. and McKenna, W. J. (2007). Desmoglein-2 mutations in arrhythmogenic right ventricular cardiomyopathy: a genotype-phenotype characterization of familial disease. *Eur. Heart J.* **28**, 581-588.

Tariq, H., Bella, J., Jowitt, T. A., Holmes, D. F., Rouhi, M., Nie, Z., Baldock, C., Garrod, D. and Tabernero, L. (2015). Cadherin flexibility provides a key difference between desmosomes and adherens junctions. *Proc. Natl. Acad. Sci. USA* **112**, 5395-5400.

Waschke, J., Spindler, V., Bruggeman, P., Zillikens, D., Schmidt, G. and Drenckhahn, D. (2006). Inhibition of Rho A activity causes pemphigus skin blistering. *J. Cell Biol.* **175**, 721-727.

Wilson, A. J., Schoenauer, R., Ehler, E., Agarkova, I. and Bennett, P. M. (2014). Cardiomyocyte growth and sarcomerogenesis at the intercalated disc. *Cell. Mol. Life Sci.* **71**, 165-181.

Zhang, Y.-M., Bo, J., Taffet, G. E., Chang, J., Shi, J., Reddy, A. K., Michael, L. H., Schneider, M. D., Entman, M. L., Schwartz, R. J. et al. (2006). Targeted deletion of ROCK1 protects the heart against pressure overload by inhibiting reactive fibrosis. *FASEB J.* **20**, 916-925.

Zhou, Y.-Q., Foster, F. S., Parkes, R. and Adamson, S. L. (2003). Developmental changes in left and right ventricular diastolic filling patterns in mice. *Am. J. Physiol. Heart Circ. Physiol.* **285**, H1563-H1575.